Geomechanics and Engineering, *Vol. 37, No. 2 (2024) 97-107*
https://doi.org/10.12989/gae.2024.37.2.097

Pile tip grouting diffusion height prediction considering unloading effect based on cavity reverse expansion model

Jiaqi Zhang[1], Chunfeng Zhao[1,2], Cheng Zhao*[1,2], Yue Wu[3] and Xin Gong[4]

[1]*Department of Geotechnical Engineering, Tongji University, Shanghai 200092, China*
[2]*Key Laboratory of Geotechnical and Underground Engineering of Ministry of Education, Tongji University, Shanghai 200092, China*
[3]*School of Civil Engineering, Chongqing Jiaotong University, 66 Xuefu Road, Chongqing 400074, China*
[4]*Institute of Civil Engineering, Jinggangshan University, Ji'an, Jiangxi 343009, China*

(*Received Spetember 18, 2022, Revised November 30, 2023, Accepted December 30, 2023*)

Abstract. The accurate prediction of grouting upward diffusion height is crucial for estimating the bearing capacity of tip-grouted piles. Borehole construction during the installation of bored piles induces soil unloading, resulting in both radial stress loss in the surrounding soil and an impact on grouting fluid diffusion. In this study, a modified model is developed for predicting grout diffusion height. This model incorporates the classical rheological equation of power-law cement grout and the cavity reverse expansion model to account for different degrees of unloading. A series of single-pile tip grouting and static load tests are conducted with varying initial grouting pressures. The test results demonstrate a significant effect of vertical grout diffusion on improving pile lateral friction resistance and bearing capacity. Increasing the grouting pressure leads to an increase in the vertical height of the grout. A comparison between the predicted values using the proposed model and the actual measured results reveals a model error ranging from -12.3% to 8.0%. Parametric analysis shows that grout diffusion height increases with an increase in the degree of unloading, with a more pronounced effect observed at higher grouting pressures. Two case studies are presented to verify the applicability of the proposed model. Field measurements of grout diffusion height correspond to unloading ratios of 0.68 and 0.71, respectively, as predicted by the model. Neglecting the unloading effect would result in a conservative estimate.

Keywords: bored piles; cavity reverse expansion; grouting diffusion; grouting pressure; post-grouting; soil unloading

1. Introduction

Cast-in-place bored piles have gained widespread use in geotechnical engineering due to their high bearing capacity, minimal settlement, and adaptability to various soil layers (Lehane *et al*. 2005, Qi *et al*. 2015, Lashkari 2017, Zou *et al*. 2019, Schmudderich *et al*. 2020, Li *et al*. 2020, Cui *et al*. 2021). During pile hole formation, soil radial unloading occurs, leading to a loss of soil stress and potentially compromising the safety of construction and the interaction between the pile and soil (Zhao *et al*. 2019). Slurry wall protection technology is commonly employed during drilling to prevent hole wall collapse (Filz *et al*. 2004, Lam *et al*. 2014, Thiyyakkandi *et al*. 2014), but it cannot fully compensate for the effects of unloading. Pile tip post-grouting, an essential engineering technique in bored pile construction, effectively addresses issues such as bearing capacity loss caused by unloading, lateral slurry cake, and bottom sediment (Saada *et al*. 2006, El-Kelesh *et al*. 2007, Chupin *et al*. 2009, Nishimura *et al*. 2011, Mozumder *et al*. 2018, Fu *et al*. 2019, Chalmovsky and Mica 2020, Zhao *et al*. 2020). The grouting process is also influenced by unloading, as cement grout injected from a tip grout outlet permeates, compacts, or splits in the surrounding soil (Ng and Lei 2003, Zhang *et al*. 2010, Thiyyakkandi *et al*. 2013, Karimi *et al*. 2017, 2018, Shrivastava and Zen 2018, Zhang *et al*. 2021). The grout accumulates at the pile tip outlet, forming a cement reinforcement block, while the remaining grout diffuses along the pile, forming reinforced cement soil and enhancing lateral resistance. Unloading creates a weak zone at the pile-soil interface, causing changes in the flow state and diffusion range of the cement grout.

Accurate prediction of grout diffusion height is a crucial step in selecting grouting parameters and estimating the ultimate bearing capacity of bored piles. However, the current determination of grout diffusion height mainly relies on personal experience, which is generally more conservative than some field observations (Zhang *et al*. 2010, Fang *et al*. 2014, 2019) and does not account for different engineering geological conditions. Therefore, the development of a well-established rational design methodology for predicting grout diffusion height is necessary to eliminate uncertainties associated with empirical methods.

In the past decade, scholars have made significant efforts to study the relationship between flow patterns, rheological parameters, and grout diffusion properties, among others, as theoretical preparations for predicting grout diffusion height. Some researchers investigated the flow pattern properties of cement grout, proposing transition points of water-cement ratio for Power-law, Bingham, and Newtonian fluids (Ruan 2005, Yang *et al*.

*Corresponding author, Professor
E-mail: zhaocheng@tongji.edu.cn

ISSN: 2005-307X (Print), 2092-6219 (Online)

2011). Rheological tests were conducted, and viscosity time-varying functions for different grouts were proposed (Ruan 2005). Yang *et al.* (2021) established a Power-law rheological equation with consideration of the comprehensive effect of time and water-cement ratio. Liu *et al.* (2018) analyzed the influence of water-cement ratio and temperature on rheological properties. It is worth noting that the grout water-cement ratios in engineering are generally between 0.5~0.7, which is regarded as the Power-law fluid (Dai *et al*. 2018, Ruan 2005). Other studies focused on grout diffusion laws in soil or rock, presenting models to evaluate grout diffusion ranges (Amadei and Savage, 2001, Bouchelaghem and Almosni, 2003, Saada *et al*. 2005, 2006, Maghous *et al*. 2007, Hou *et al*. 2019, Jafarpour *et al*. 2020, Huang *et al*. 2020). These investigations into grout rheological properties and diffusion laws laid the foundation for theoretical research on grout diffusion height in piles.

Regarding the theory of grout diffusion height, previous studies by Zhang *et al.* (2010) and Fang *et al.* (2019) proposed prediction approaches for the returned height of pile tip grouting by incorporating grout flow equations and cavity expansion theory, respectively. Zhang's analysis further demonstrated that grouting pressure, pile buried depth, pile diameter, and slurry cake thickness all influence the grouting height. Considering the time-dependent viscosity behaviors of Power-law grout, Dai *et al.* (2018) and Zhang *et al*. (2021) improved the computational methods for grout diffusion height. However, these existing studies have not taken into account the influence of unloading on soil displacement, thus limiting their applicability to bored piles. El Jirari *et al*. (2020) and Zhao *et al.* (2023) investigated the reverse expansion behavior of cavities after unloading based on Tresca and Mohr-Coulomb criteria, respectively. These studies have laid the groundwork for establishing a grout diffusion model that considers the effect of unloading.

Based on the aforementioned analysis, this study proposes a Power-law model for grout diffusion in pile tip grouting, which incorporates the consideration of the unloading effect. To verify the applicability of the model, a series of single pile grouting and static load model tests, as well as two field cases documented in the literature, were conducted. Furthermore, the study examines the impact of unloading degree and grouting pressure on the diffusion range.

2. Pile tip grouting diffusion height model

2.1 Assumptions

In the development of the grout diffusion height model, certain fundamental assumptions are made regarding the pile and grout characteristics. These assumptions are as follows:

(1) Elastic-plastic radial soil unloading occurs around the pile as a result of the drilling process. The unloading ratio, denoted as $\chi = P_u/P_0$, represents the ratio of the soil stress reduction caused by unloading. The horizontal soil stress after unloading at the drilling wall is represented by P_u, while P_0 represents the initial horizontal soil stress. The value of χ remains constant with increasing depth.

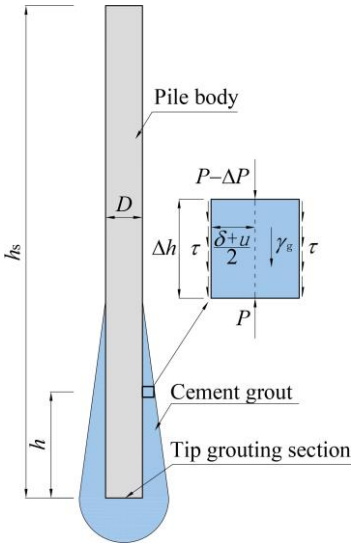

Fig. 1 Schematic of pile tip grouting diffusion

(2) The utilization of slurry wall protection technology leads to the formation of a slurry cake layer with a uniform thickness along the pile-soil interface.

(3) The cement grout used in the study is considered to be a Power-law fluid with a water-cement ratio ranging from 0.5 to 0.7, as supported by previous research (Ruan 2005, Zhang *et al*. 2010).

(4) The extrusion displacement of grout split on the soil is small. Therefore, the cylindrical borehole around the pile in the grout diffusion sections is assumed to be in a state of reverse elastic expansion (Zhang *et al*. 2010, Dai *et al*. 2018). Specifically, for pile tip grouting, the grout splits along the weak interface between the pile and soil from the grout outlet, forming a reinforced ring zone, as illustrated in Fig. 1.

In reality, a grout bubble will be formed at the pile tip grouting outlet, and the soil near the pile tip is often in a plastic state. As the grout pressure decreases, the soil in the diffusion range further away from the pile tip transitions into a state of reverse elasticity. Therefore, assumption (4) is made as a simplification to determine the grout diffusion height.

2.2 Soil reverse expansion displacement

Before grouting, the soil surrounding a pile is in a state of radial unloading. The degree of unloading in soil χ is influenced by the construction method employed for cast-in-place piles. In the case of the dry operation method, the value of χ can be assigned as 0. However, for piles incorporating slurry wall protection technology, the value of χ is typically determined by considering factors such as the lateral pressure exerted by the slurry and the type of soil. This determination is based on relevant studies conducted by Al-Ajmi and Zimmerman (2006), and Gholami *et al*. (2014).

Taking the vertical position of a tip grout outlet as the origin of computation, at a vertical distance h from the grout outlet, the horizontal soil stress after unloading at the drilling wall can be expressed as follows

$$P_{\mathrm{u}}(h)=\chi P_0(h)=\chi K_0\left(\gamma_{\mathrm{m1}}h_{\mathrm{s}}-\gamma_{\mathrm{m2}}h\right) \tag{1}$$

where K_0 is static soil pressure coefficient. The classical formula can be introduced: K_0=1-sinφ, φ is internal friction angle. h_{s} is the distance from the grout outlet to the soil surface. γ_{m1} is the average soil weight in the range of h_{s}. And γ_{m2} is the average soil weight from the grout outlet to the computed point.

In the grouting process, grout pressure at height h in grout is $P(h)$. Especially at the grout outlet, the initial grouting pressure

$$P(0)=P_{\mathrm{s}} \tag{2}$$

During the drilling stage, the unloading of soil around piles is commonly simulated using cylindrical cavity contraction. Based on this contraction process, the extrusion of grout splitting on the soil can be understood as an elastic reverse expansion. Extensive research has been conducted by scholars on models of cavity expansion and reverse expansion considering unloading(Zhao *et al*. 2023, El Jirari *et al.* 2020, Li *et al*. 2021, Li *et al*. 2016, Silvestri and Abou-Samra 2012). Drawing from Zhao's cylindrical reverse expansion model, which includes an elastic phase displacement formula (Eq. (10) in Zhao *et al*. 2023), the reverse radial displacement of soil at the pile-soil interface at a height h can be expressed as follows

$$u(h)=\frac{\left[P(h)-P_{\mathrm{u}}(h)\right]}{2G}\left(\frac{D}{2}+\delta+u(h)\right) \tag{3}$$

Arrange Eq. (3) to get

$$u(h)=\frac{\left[P(h)-P_{\mathrm{u}}(h)\right]\left(\frac{D}{2}+\delta\right)}{2G+P_{\mathrm{u}}(h)-P(h)} \tag{4}$$

$$G=\frac{E}{2(1+\nu)} \tag{5}$$

Where u is reverse radial displacement, D is pile diameter, δ is slurry cake thickness, E is soil elastic modulus, ν is Poisson's ratio, and G is soil shear modulus.

2.3 Grout flow equation

In pile grouting engineering, a commonly used rheological equation of power-law cement grout (Zhang *et al*. 2010, Dai *et al*. 2018, Fang *et al*. 2019, Zhang *et al*. 2021) is to describe the relationship between grout shear stress and flow velocity

$$\tau=k\gamma^n \tag{6}$$

$$\gamma=-\frac{\mathrm{d}v}{\mathrm{d}y} \tag{7}$$

Where τ is grout shear stress, k is consistency coefficient, n is a rheological index, γ is shear rate, v is grout flow velocity, and y is the radial distance between the computed point and grout center.

As shown in Fig. 1, considering a grout cross-section of height difference Δh, it can be considered as a narrow rectangular slit when Δh is small. Bathed on the equilibrium condition, the uniform grout diffusion flow equation can be obtained as follows

$$\tau=\left(\frac{\Delta P}{\Delta h}-\gamma_{\mathrm{g}}\right)y \tag{8}$$

Where ΔP is the pressure difference between the upper and lower grout section, and γ_{g} is grout weight.

At the section edge

$$v\Big|_{y=\frac{\delta+u}{2}}=0 \tag{9}$$

Combine Eqs. (6)-(9) and integrate it

$$v=\frac{n}{n+1}\left(\frac{1}{k}\right)^{\frac{1}{n}}\left(\frac{\Delta P}{\Delta h}-\gamma_{\mathrm{g}}\right)^{\frac{1}{n}}\left[\left(\frac{\delta+u}{2}\right)^{\frac{n+1}{n}}-y^{\frac{n+1}{n}}\right] \tag{10}$$

Considering a complete grout ring with a height difference Δh, the flow rate q of cement grout in unit time is

$$\begin{aligned}q&=\int_{-\frac{\delta+u}{2}}^{\frac{\delta+u}{2}}v\pi(D+\delta+u)\mathrm{d}y\\&=2\pi(D+\delta+u)\int_0^{\frac{\delta+u}{2}}v\mathrm{d}y\\&=\frac{2n\pi(D+\delta+u)}{2n+1}\left(\frac{1}{k}\right)^{\frac{1}{n}}\left(\frac{\Delta P}{\Delta h}-\gamma_{\mathrm{g}}\right)^{\frac{1}{n}}\left(\frac{\delta+u}{2}\right)^{\frac{2n+1}{n}}\end{aligned} \tag{11}$$

Eq. (11) can be deformed to obtain the pressure difference

$$\Delta P=\left\{\left(\frac{2n+1}{n}\right)^n\left[\frac{q}{\pi(D+\delta+u)}\right]^n\frac{2^{n+1}k}{(\delta+u)^{2n+1}}+\gamma_{\mathrm{g}}\right\}\Delta h \tag{12}$$

2.4 Solution of grout diffusion height

During the grouting stage, the grout pressure gradually decreases with increasing distance from the grout outlet due to the effect of shear forces. As long as the grout pressure remains higher than the splitting threshold, which is the horizontal soil stress, the grout is capable of spreading along the pile-soil interface. Eventually, the grout reaches its ultimate upward diffusion height

$$P\Big|_{h=h_{\mathrm{u}}}=P_u(h) \tag{13}$$

Where h_{u} is the ultimate upward diffusion height.

The solution process of the ultimate grout diffusion height can be summarized as follows:

(1) Determine basic physical parameters of soil layers, pile size, and grouting parameters.

Table 1 Soil parameters of the model test

Elastic modulus (MPa)	Poisson's ratio	Cohesion (kPa)	Internal friction angle (°)	Density (kg·m^{-3})
6.07	0.3	16.2	16.7	1870

(2) Based on the depth distribution of soil layers, set a height difference Δh from the grout outlet or a computed point. Then, combine Eqs. (1)-(5) and (12) to compute the grout pressure reduction ΔP of this section.

(3) Determine whether $P(h) \leq P_u(h)$ is true at the computed point, if the inequality is true, then h is h_u; If not, repeat (2) and (3) until the inequality is true. Particularly, if $h_u > h_s$, grout overflow at the pile top will occur.

3. Single pile grouting and static load model test

3.1 Test scheme

3.1.1 Model piles

To validate the proposed model for pile tip grouting diffusion height, a single pile grouting and vertical compression static load test was conducted. The influence of initial grouting pressure on both grout diffusion height and pile lateral resistance was also investigated. The model test took place at the Key Laboratory of Geotechnical and Underground Engineering of Tongji University, within a large chamber (Wu *et al*. 2023, Zhao *et al*. 2020, Zhang *et al*. 2023). The test utilized soil samples obtained from a cohesive soil layer at an engineering site in Shanghai, China, with specific parameters listed in Table 1. The geometric similarity ratio of the model test is 26.

In the test setup, a prefabricated model pile was constructed, consisting of an inner pile core, an outer cement mortar pile body, and a tip grouting pipe, closely resembling a reinforced concrete pile. The diameter of the pile was 46 mm, and its dimensions are illustrated in Fig. 2.

The pile core was fabricated using L-shaped aluminum, and strain gauges were symmetrically attached to the pile at specific distances to monitor strain variations. The tip grouting pipe, made of seamless steel tubes, was embedded in the pile core. The design buried depth of model piles is 1.8 m. To simulate practical engineering drilling and soil unloading scenarios, PVC pipes were initially embedded in the soil. Subsequently, the PVC pipes were replaced with the model piles. After a period of natural static consolidation lasting several months, during which the horizontal soil pressure partially recovered, a certain degree of unloading was formed. To account for the influence of the slurry cake on grout diffusion, a thin slurry layer was applied to the surface of each pile before filling.

3.1.2 Test groups

In order to validate the proposed model outlined in this paper, a series of four pile tests were conducted. These tests consisted of one non-grouting pile (N00) and three tip grouting piles (T25, T26, and T27), as documented in Table 2. Considering the size of the model piles and previous test experiences (Zhao *et al*. 2020), the total grout volume for each model pile is 2 L. In post-grouting projects, the grouting pressure is generally kept below 6 MPa. According to the principle of similarity, the grouting pressure in the model tests should be around 0.2 MPa. However, based on preliminary experimental results, the selected cohesive soil only exhibits injectability at grouting pressures above 0.5 MPa. Therefore, for the three grouted piles in the test, the initial grouting pressures chosen were 0.5 MPa, 0.6 MPa, and 0.7 MPa, respectively.

Table 2 Grouting parameters and ultimate bearing capacities of model piles

Pile number	N00	T25	T26	T27
Grout volume (L)	0	2	2	2
Initial grouting pressure (MPa)	-	0.5	0.6	0.7
Ultimate bearing capacity (kN)	0.8	4.8	3.4	6.0

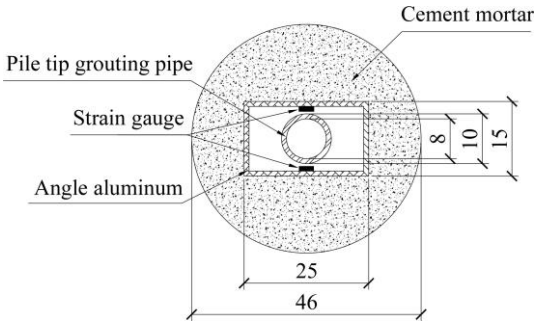

Fig. 2 Model pile section

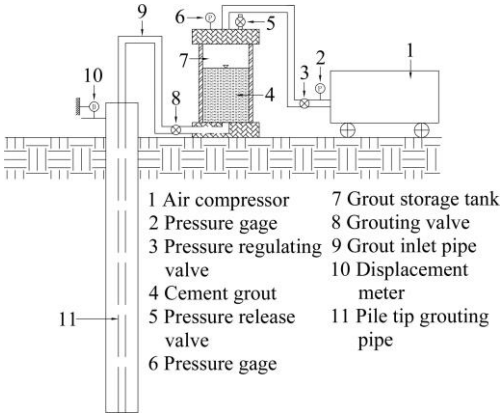

Fig. 3 Schematic of grouting device

3.1.3 Grouting and loading

In this test, a grout mixture consisting of ordinary Portland cement (P.O) 42.5 and a water-cement ratio of 0.6 was selected as the grouting material taking into account the strength of the grouted soil and the workability of the grout. The grouting equipment utilized consisted of an air compressor, pressure regulating valves, a grout storage tank, a grout inlet pipe, a pressure gauge, and other components, as depicted in Fig. 3. By manipulating the pressure regulating valve, compressed air at a specific

pressure was introduced into the grout storage tank and a defined volume of cement grout was subsequently injected into the grouting pipe.

The loading procedure employed in the test involved converting the weight of specific loads into a vertical load applied to the top of the pile achieved through the use of steel tracks and pulley blocks. The schematic diagram of the loading device can be referenced from Fig. 7 in the study by Wu *et al.* (2023). Throughout the loading process, dial gauges were employed to measure the settlement of the pile cap, while strain gauges were utilized to capture the deformations of the pile body. The loading process followed the rapid maintenance load method prescribed in the Chinese code (2014). The criterion for terminating the loading process is based on observing that the displacement at the pile top under a specific load level exceeds 5 times that of the preceding level. The ultimate bearing capacity of the model pile is determined by the load value achieved in the previous stage.

3.2 Test results and analysis

3.2.1 Bearing capacities and lateral friction resistances of model piles

Based on the test results, the vertical ultimate bearing capacities of the four model piles are presented in Table 2. The non-grouting pile exhibited an ultimate bearing capacity of 0.8 kN, whereas the other three grouting piles demonstrated capacities exceeding 3.4 kN. Following grouting, the enhancement ratios ranged from 325% to 650%, which exceeded typical field test results (Cai *et al*. 2012, Liu *et al*. 2013, Cui *et al*. 2021). Upon analyzing the reasons, it was found that the pile side unloading and slurry setting during the test resulted in a significant weakening of skin friction in the case of the non-grouting pile (N00), thereby diminishing its lateral friction resistance and bearing capacity. Conversely, the reinforcing effect of grouting on the soil surrounding the piles became highly pronounced in the scale test conducted under low soil pressure conditions. Based on the test results, it can be observed that as the grouting pressure increases from 0.5 MPa to 0.6 MPa and 0.7 MPa, the ultimate bearing capacity initially decreases and then increases. Therefore, it is difficult to directly determine the optimal pressure. This fluctuation in results may be attributed to the relatively small pressure gradient, which leads to significant variations.

Fig. 4 illustrates the distribution of ultimate lateral resistance for each model pile. As shown, N00 exhibited low average pile lateral resistance throughout each section, with the maximum lateral resistance reaching only 2.9 kPa. In contrast, the lateral friction distribution for the tip-grouted piles exhibited clear regularity, with sections near the grout outlet experiencing significant enhancement, reaching a maximum of 39.5 kPa in the case of T27. The lateral resistance of pile T26 within the range of 1.50 m to 1.75 m is 22.2 kPa, which is significantly lower compared to piles T25 and T27. The lateral resistances of sections located far from the grout outlet in the grouted piles were comparable to those of the non-grouting pile. The enhanced

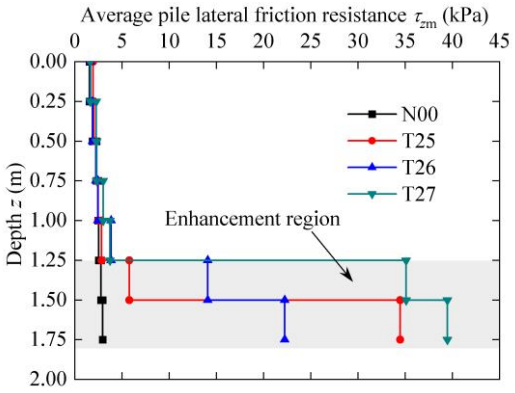

Fig. 4 Ultimate lateral resistances of model piles

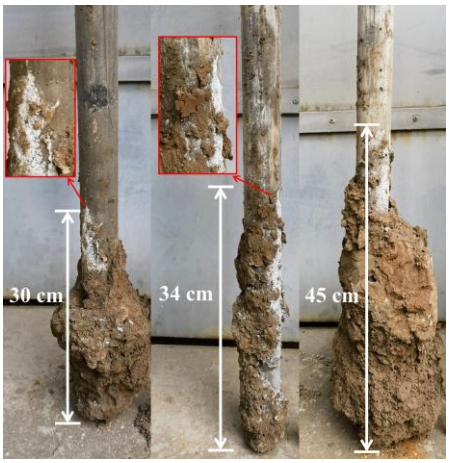

Fig. 5 Measurement of grouting diffusion height of model piles

region of lateral friction resistance was observed within the depth range of 1.25 to 1.75 m. This phenomenon of increased lateral resistance indicated effective filling of the pile-soil interface by the cement grout along the pile body. For each grouting condition, the degree of skin friction enhancement decreased with increasing distance from the grout outlet.

After completing the experiment, the model piles were excavated from the test chamber. The measurement results of the ultimate vertical diffusion range of grout in each tip-grouted pile under different grouting pressures are presented in Fig. 5. From the perspective of grout failure mode, a significant portion of grout failure in pile T26 occurs between the grout and the pile. On the other hand, the remaining two piles primarily exhibit failure between the grout and the soil, thereby preserving a relatively intact grout body. This also explains the reason that the lateral resistance of pile T26 in the reinforced area is smaller compared to piles T25 and T27. Significantly, the diffusion height of grout in tip-grouted piles exhibits notable variation depending on the grouting pressure applied. Specifically, at grouting pressures of 0.5, 0.6, and 0.7 MPa, the upward diffusion heights of grout are measured as 30 cm, 34 cm, and 45 cm, respectively. This observed trend roughly corresponds to the enhancement range of lateral friction resistance.

Table 3 Comparison of measured and computed grouting diffusion heights of model piles

Pile number	T25	T26	T27
Measured height (cm)	30	34	45
Computed height (cm)	26.3	36.5	48.6
Error (%)	-12.3	7.4	8.0

3.2.2 Model parameters

In this reduced-scale test, the soil surrounding the pile experienced complete unloading during the filling process of prefabricated piles. As the construction process of the model piles can be considered a dry operation method, the soil unloading ratio χ is 0. In this analysis, the influence of soil stress recovery resulting from soil consolidation is disregarded, because the unloading ratio has little effect on the model test with shallow soil depth. In fact, compared to complete unloading, the maximum decrease in grout diffusion height in theoretical computations is only 0.01 m when the unloading ratio χ equals 1 in the test. The slurry cake has an approximate thickness of 0.5 mm. The weight of the cement grout is 17 kN/m^{-3}. Based on the actual grouting speed, the flow rate q is set at 0.2 L/s. The rheological parameters of the cement grout can be determined using prior research findings on power-law cement grout, specifically the work conducted by Ruan (2005). In Ruan's study on the rheological characteristics of grout, the consistency coefficient $k = 8.632$, and the rheological index $n = 0.0026$.

3.2.3 Comparison between test and model results of grouting diffusion height

Table 3 provides a comparison between the measured and computed grouting diffusion heights of the model piles. Relative to the testing results, the error range of the theoretical solution falls between -12.3% to 8.0%. It is important to note that the grouting details and soil conditions of each pile may not be entirely consistent, which accounts for the observed discrepancies. Nonetheless, the overall comparison results generally validate the effectiveness of the proposed model.

Regarding post-grouting, higher grouting pressures lead to an increase in the grout diffusion range. This is due to the increased distance required to reduce the grout pressure to the splitting threshold. Therefore, in post-grouting engineering, it is crucial to ensure both the initial value and stability of the grouting pressure.

4. Analysis of unloading effect and grouting pressure on grout diffusion height

The shallow burial depth of piles in the model test shows a relatively minor unloading effect on grout diffusion. However, in practical pile engineering, soil stress is typically high, and significant soil pressure unloading can have a noticeable impact on grout diffusion.

In this section, an example is presented to discuss the influence of the unloading effect on the grout diffusion

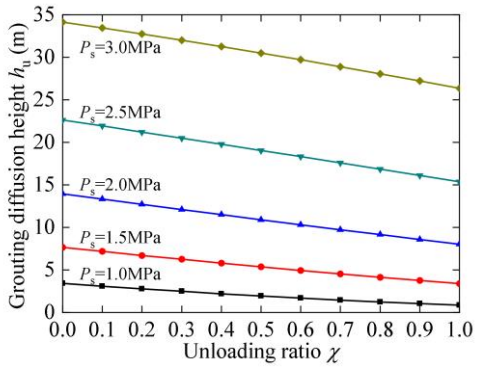

Fig. 6 Variation of grout diffusion height with different unloading ratios

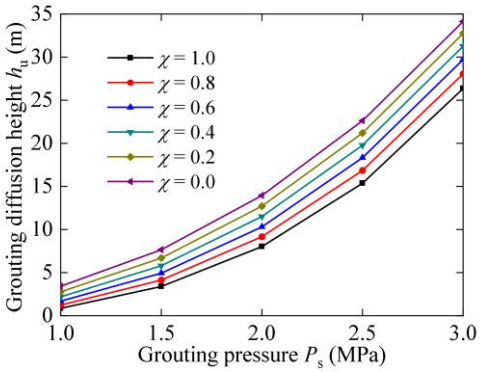

Fig. 7 Variation of grout diffusion height with different grouting pressures

range. The parameters of the clay layer specified in Table 1 are adopted, with a pile diameter $D = 1$ m. The depth of the tip grouting outlet h_s=40 m, and the thickness of the slurry cake $\delta = 0.01$ m. The grouting parameters are set as follows: grouting pressure P_s =1~3 Mpa, q=0.2 L/s.

Fig. 6 illustrates the variation curves of pile tip grouting diffusion heights under different unloading ratios and initial grouting pressures. With a fixed grouting pressure, the grout diffusion range expands as the unloading ratio decreases, and the relationship between diffusion height and unloading ratio shows a close-to-linear trend. This indicates a positive effect of unloading on grout diffusion. For instance, at a grouting pressure of 1.0 MPa, as the unloading ratio decreases from 1 to 0, the diffusion height increment is 2.56 m (from 0.86 m to 3.42 m). Conversely, when the grouting pressure is 3 MPa, complete unloading is expected to result in an increase in diffusion height from 26.36 m to 34.13 m, yielding a height increment of 7.77 m. The influence of unloading on grout diffusion height becomes more significant with increasing grouting pressure, as demonstrated by the variation curve presented in Fig. 7. The diffusion height exhibits a clear increasing trend with higher grouting pressure, and at elevated pressures, the diffusion height becomes more sensitive to pressure changes.

Based on the aforementioned analysis, it is evident that the unloading effect positively impacts grout diffusion. Thus, it is conservative not to consider unloading when determining the grouting reinforcement region for predicting and designing the bearing capacity of bored

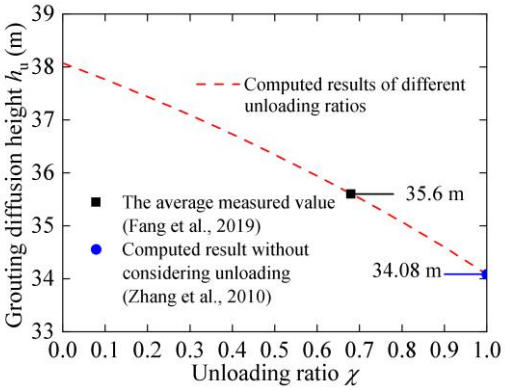

Fig. 8 Comparison between measured and computed grout diffusion heights of Case 1

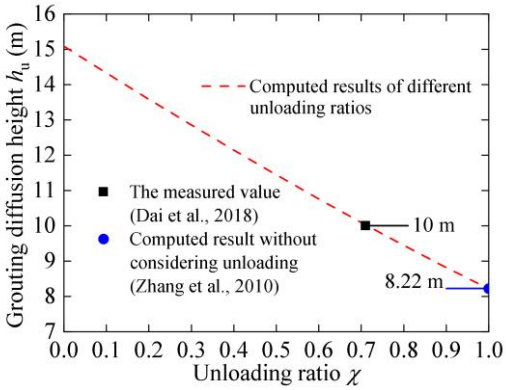

Fig. 9 Comparison between measured and computed grout diffusion heights of Case 2

piles. In post-grouting projects, it is crucial to maintain a high and stable grouting pressure to ensure sufficient grouting reinforcement at the pile-soil interface.

5. Model application and validation

5.1 Case 1

A field test was conducted by Fang *et al.* (2019) on tip-grouted piles with a diameter of 0.8 m and a length of 40 m. The soil layer parameters at the field site are presented in Table 4. During the test, cement grout with a water-cement ratio of 0.6 and a unit weight of 16.9 kN/m^3 was utilized. The grouting pressure at the pump was approximately 3 MPa, while the pressure at the pile tip, as measured by a pressure gauge, was around 1.2 MPa. The grout injection rate employed was approximately 0.003 m^3/s.

A total of 8 piles were included in the field test. With the exception of two situations—one where grout overflowed to the surface and another where one pile was excavated to a depth of 8 m underground without detecting the cement layer—the grout diffusion height of the remaining 6 piles ranged from 32.6 m to 38.3 m, with an average value of 35.6 m. Fig. 8 presents a comparison between the measured and computed grout diffusion heights. As the unloading ratio decreases from 1 to 0, the computed diffusion height falls within the range of 34.08 m to 38.07 m. The measured height values generally align with the computed range. In terms of the unloading ratio, the average measured value corresponds to the position of χ =0.68 on the diffusion height curve. If unloading is not taken into account, the computed result is 34.08 m (Zhang *et al*. 2010), which is approximately 1.52 m lower than the average measured value.

5.2 Case 2

Dai *et al.* (2018) reported a field test on a tip-grouted pile foundation of a bridge pier with a diameter of 1.5 m and a length of 56 m. The soil parameters surrounding the pile are presented in Table 5. During the post-grouting process, the cement grout had a water-cement ratio of 0.5. The grouting pressure applied was 1.588 MPa, and the grout injection rate was approximately 0.0016 m^3/s. In the model calculation, the rheological parameters of the grout were selected to be consistent with Dai's study: $k = 45$ Pa·s and $n = 0.15$.

Fig. 9 illustrates the comparison between the measured and computed grout diffusion heights. The measured grout diffusion height was approximately 10 m. In the computed results presented in this paper, as the unloading ratio decreases from 1 to 0, the computed diffusion height falls within the range of 8.22 m to 15.09 m. The measured value corresponds to the position of χ =0.71 on the diffusion height curve. In comparison to the measured value, Zhang's solution (Zhang *et al.* 2010) yields a computed diffusion height of 8.22 m, which is approximately 1.78 m lower than the measured value.

5.3 Discussion

The applicability of the model is demonstrated through the comparison of computed results with measurements from two field tests. These measurements correspond to calculated values at unloading ratios of 0.68 and 0.71 in the model, indicating that the unloading ratio for grouted piles utilizing slurry wall technology is approximately 0.7. When calculating the grout diffusion height at the pile tip, the unloading ratio of the soil can be estimated based on the slurry density and soil parameters. In the absence of construction and soil data or for quick estimations, an unloading ratio of 0.7 can be used to estimate the grout diffusion height.

6. Conclusions

In this study, authors have developed a theoretical model for predicting the grout diffusion height at the tip of a pile, taking into consideration the unloading effect. The influence of the unloading ratio and grouting pressure on the grout diffusion height has been thoroughly analyzed through model tests and parameter studies. In addition, the accuracy of this model is verified by a laboratory test and two field cases. The key findings of this research are as follows:

Table 4 Soil properties of the test site of Case 1

Type of soil layer	Thickness (m)	Unit weight (kN/m^3)	Compression Modulus (MPa)	Coefficient of lateral pressure
Fill	4.5	17.5	7.9	0.40
Sandy silt	2.9	18.6	11.5	0.40
Sandy silt	2.8	18.8	11.8	0.41
Sandy silt	2.3	18.8	10.8	0.41
Silty sand	3.8	19.1	11.3	0.33
Silty clay	7.1	17.3	3.3	0.56
Silty clay	2.2	18.8	6.5	0.47
Silty clay	2.8	19.2	7.0	0.46
Fine sand	7.0	19.7	8.6	0.36
Gravel	16.7	20	—	—

Table 5 Soil properties of the test site of Case 2

Type of soil layer	Thickness (m)	Unit weight (kN/m^3)	Compression Modulus (MPa)	Coefficient of lateral pressure
Fill	1.0	—	—	—
Silty clay	0.9	18.23	4.24	0.54
Mucky clay	5.2	17.54	3.08	0.72
Mucky clay	6.5	16.95	2.31	0.72
Mucky silty clay	5.2	17.64	2.85	0.67
Silt	8.2	18.82	8.48	0.33
Clay	8.1	18.42	3.98	0.54
Silty clay	5.9	18.72	4.17	0.43
Silty clay	10.1	18.33	6.03	0.43
Silt	1.5	18.13	9.29	0.33
Silty clay	3.4	19.40	5.00	0.43

(1) After pile tip grouting, a distinct vertical diffusion area is formed, resulting in a significant increase in lateral friction resistance and, consequently, the overall bearing capacity. When comparing the predicted values from our model with actual measurements, the model error falls within the range of -12.3% to 8.0%. It is evident that the grout diffusion height exhibits a clear positive correlation with the grouting pressure.

(2) The grout diffusion height increases as the unloading ratio decreases. The relationship between the grout height and unloading ratio can be approximated as linear. Moreover, the impact of unloading becomes more pronounced as the grouting pressure rises. At higher grouting pressures, the diffusion height becomes more sensitive to changes in pressure.

(3) Two case studies were conducted to validate the applicability of the proposed model. The field measurements of the grout diffusion height correspond to unloading ratios of 0.68 and 0.71, respectively, as predicted by the model. If the unloading effect is disregarded, the predicted height would be conservative and underestimated by approximately 1.52~1.78 m.

Acknowledgments

The authors are deeply grateful for the financial support of the National Natural Science Foundation of China (Grant Nos. 42377151, and 02302340428), the Natural Science Foundation of Chongqing (CSTB2023NSCQ-BHX0149), the China Postdoctoral Science Foundation (2023MD734112). The comments of the anonymous reviewers have improved the quality of this paper and are also gratefully acknowledged.

References

Al-Ajmi, A.M. and Zimmerman, R.W. (2006), "Stability analysis of vertical boreholes using the Mogi-Coulomb failure criterion", *Int. J. Rock Mech. Min. Sci.*, **43**(8), 1200-1211. https://doi.org/10.1016/j.ijrmms.2006.04.001.

Amadei, B. and Savage, W.Z. (2001), "An analytical solution for transient flow of Bingham viscoplastic materials in rock fractures", *Int. J. Rock Mech. Min. Sci.*, **38**(2), 285-296. https://doi.org/10.1016/s1365-1609(00)00080-0.

Bouchelaghem, F. and Almosni, A. (2003), "Experimental determination of the longitudinal dispersivity during the injection of a micro-cement grout in a one-dimensional soil

column", *Transport in Porous Media*, **52**(1), 67-94. https://doi.org/10.1023/a:1022376225651

Cai, J., Wang, Y.Y., Wang, X.H. and Yan, H.W. (2012), "Evaluation on bearing capacity improvement of cast-in-situ bored piles using post-grouting technology", *Proceedings of* the *International Conference on Civil, Architectural and Hydraulic Engineering (ICCAHE 2012)*, August 10-12, Zhangjiajie, Hunan, China.

Chalmovsky, J. and Mica, L. (2020), "Prediction of the load-displacement response of ground anchors via the load-transfer method", *Geomech. Eng.*, **20**(4), 359-370. https://doi.org/10.12989/gae.2020.20.4.359.

Chupin, O., Saiyouri, N. and Hicher, P.Y. (2009), "Modeling of a semi-real injection test in sand", *Comput.Geotech.*, **36**(6), 1039-1048. https://doi.org/10.1016/j.compgeo.2009.03.014.

Cui, Y.L., Qi, C.G., Zheng, J.H., Wang, X.Q. and Zhang, S.M. (2021), "Field test research on post-grouting effect for super-long cast-in-place bored pile in thick soft foundation", *Geotech. Geol. Eng.*, **39**(7), 4833-4842. https://doi.org/10.1007/s10706-021-01796-x

Dai, G.L., Wan, Z.H., Zhu, M.X. and Gong, W.M. (2018), "The model of grout migration height for pressured grouting at pile tip based on time-dependent behavior of viscosity and its engineering application", *Rock Soil Mech*., **39**(8), 2941-2950. https://doi.org/10.16285/j.rsm.2018.0588. (in Chinese)

El Jirari, S., Wong, H., Deleruyelle, F., Branque, D., Berthoz, N. and Leo, C. (2020), "Analytical modelling of a tunnel accounting for elastoplastic unloading and reloading with reverse yielding and plastic flow", *Comput. Geotech.*, **121**, 103441. https://doi.org/10.1016/j.compgeo.2020.103441.

El-Kelesh, A.M., Matsui, T. and Tokida, K. (2007), "Field investigation into effectiveness of shallow treatment by compaction grouting", *Proceedings of the 17th International Offshore and Polar Engineering Conference (ISOPE 2007)*, July 01-06, Lisbon, Portugal.

Fang, K., Zhang, Z.M. and Yang, Q.D. (2014), "Response evaluation of axially loaded grouted drilled shaft", *Mar. Georesour. Geotec.*, **32**(2), 123-134, https://doi.org/10.1080/1064119x.2012.710713.

Fang, K., Zhao, T.B., Tan, Y.L. and Qiu, Y. (2019), "Prediction of grouting penetration height along the shaft of base grouted pile", *J. Mar. Sci. Eng.*, **7**(7), 212. https://doi.org/10.3390/jmse7070212.

Filz, G.M., Adams, T. and Davidson, R.R. (2004), "Stability of long trenches in sand supported by bentonite-water slurry", *J. Geotech. Geoenviron. Eng.*, **130**(9), 915-921. https://doi.org/10.1061/(asce)1090-0241(2004)130:9(915).

Fu, Y.B., Wang, X.L., Zhang, S.Z. and Yang, Y. (2019), "Modelling of permeation grouting considering grout self-gravity effect: theoretical and experimental study", *Adv. Mater. Sci. Eng.*, **2019**, 7968240. https://doi.org/10.1155/2019/7968240.

Gholami, R., Moradzadeh, A., Rasouli, V. and Hanachi, J. (2014), "Practical application of failure criteria in determining safe mud weight windows in drilling operations", *J. Rock Mech. Geotech. Eng.*, **6**(1), 13-25.

Hou, F.J., Sun, K.G., Wu, Q.D., Xu, W.P. and Ren, S.J. (2019), "Grout diffusion model in porous media considering the variation in viscosity with time", *Adv. Mech. Eng.*, **11**(1), 1-9. https://doi.org/10.1177/1687814018819890.

Huang, S.L., Pei, Q.T., Ding, X.L., Zhang, Y.T., Liu, D.X., He, J. and Bian, K. (2020), "Grouting diffusion mechanism in an oblique crack in rock masses considering temporal and spatial variation of viscosity of fast-curing grouts", *Geomech. Eng.*, **23**(2), 151-163. https://doi.org/10.12989/gae.2020.23.2.151.

Jafarpour, P., Moayed, R.Z. and Kordnaeij, A. (2020), "Behavior of zeolite-cement grouted sand under triaxial compression test", *J. Rock Mech. Geotech. Eng.*, **12**(1), 149-159. https://doi.org/10.1016/j.jrmge.2019.06.010.

Karimi, A.H., Eslami, A., Zarrabi, M. and Khazaei, J. (2017), "Study of pile behavior by improvement of confining soils using frustum confining vessel", *Scientia Iranica*, **24**(4), 1874-1882. https://doi.org/10.24200/sci.2017.4278.

Karimi, A.H. and Eslami, A. (2018), "Physical modelling for pile performance combined with ground improvement using frustum confining vessel", *Int. J. Phys. Model. Geotech.*, **18**(3), 162-174. https://doi.org/10.1680/jphmg.15.00038.

Lam, C., Jefferis, S.A. and Martin, C.M. (2014), "Effects of polymer and bentonite support fluids on concrete-sand interface shear strength", *Geotechnique*, **64**(1), 28-39. https://doi.org/10.1680/geot.13.P.012.

Lashkari, A. (2017), "A simple critical state interface model and its application in prediction of shaft resistance of non-displacement piles in sand", *Comput. Geotech.*, **88**, 95-110. https://doi.org/10.1016/j.compgeo.2017.03.008.

Lehane, B.M., Gaudin, C. and Schneider, J.A. (2005), "Scale effects on tension capacity for rough piles buried in dense sand", *Geotechnique*, **55**(10), 709-719. https://doi.org/10.1680/geot.2005.55.10.709.

Li, L., Chen, H.H., Li, J.P. and Sun, D.A. (2021), "An elastoplastic solution to undrained expansion of a cylindrical cavity in SANICLAY under plane stress condition", *Comput. Geotech.*, **132**, 103990. https://doi.org/10.1016/j.compgeo.2020.103990.

Li, L., Li, J.P. and Sun, D.A. (2016), "Anisotropically elasto-plastic solution to undrained cylindrical cavity expansion in K-0-consolidated clay", *Comput. Geotech.*, **73**, 83-90. https://doi.org/10.1016/j.compgeo.2015.11.022.

Li, L., Li, J.P., Wang, Y. and Gong, W.B. (2020), "Analysis of nonlinear load-displacement behaviour of pile groups in clay considering installation effects", *Soils Found.*, **60**(4), 752-766. https://doi.org/10.1016/j.sandf.2020.04.008.

Liu, N.W., Zhang, Z.M., Zhang, Q.Q. and Fang, K. (2013), "Destructive field tests on mobilization of end resistance of cast-in-situ bored piles", *J. Central South Univ.*, **20**(4), 1071-1078. https://doi.org/10.1007/s11771-013-1586-8.

Liu, Q.S., Lei, G.F., Peng, X.X., Lu, C.B. and Wei, L. (2018), "Rheological characteristics of cement grout and its effect on mechanical properties of a rock fracture", *Rock Mech. Rock Eng.*, **51**(2), 613-625. https://doi.org/10.1007/s00603-017-1340-x.

Maghous,. S, Saada, Z., Dormieux, L., Canou, J. and Dupla, J.C. (2007), "A model for in situ grouting with account for particle filtration", *Comput. Geotech.*, **34**(3), 164-174. https://doi.org/10.1016/j.compgeo.2006.11.003.

Mozumder, R.A., Laskar, A.I. and Hussain, M. (2018), "Penetrability prediction of microfine cement grout in granular soil using Artificial Intelligence techniques", *Tunn. Undergr. Sp. Tech.*, **72**, 131-144. https://doi.org/10.1016/j.tust.2017.11.023.

Ng, C.W.W. and Lei, G.H. (2003), "Performance of long rectangular barrettes in granitic saprolites", *J. Geotech. Geoenviron. Eng.*, **129**(8), 685-696. https://doi.org/10.1061/(asce)1090-0241(2003)129:8(685).

Nishimura, S., Takehana, K., Morikawa, Y. and Takahashi, H. (2011), "Experimental study of stress changes due to compaction grouting", *Soils Found.*, **51**(6), 1037-1049. https://doi.org/10.3208/sandf.51.1037.

Qi, C.G., Liu, G.B., Wang, Y. and Deng, Y.B. (2015), "A design method for plastic tube cast-in-place concrete pile considering cavity contraction and its validation", *Comput. Geotech.*, **69**, 262-271. https://doi.org/10.1016/j.compgeo.2015.05.016.

Ruan, W.J. (2005), "Research on diffusion of grouting and basic properties of grouts", *Chinese J. Geotech. Eng.*, **27**(1), 69-73. (in Chinese)

Saada, Z., Canou, J., Dormieux, L., Dupla, J.C. and Maghous, S.

(2005), "Modelling of cement suspension flow in granular porous media", *Int. J. Numer. Anal. Method. Geomech.*, **29**(7), 691-711. https://doi.org/10.1002/nag.433.

Saada, Z., Canou, J., Dormieux, L. and Dupla, J.C. (2006), "Evaluation of elementary filtration properties of a cement grout injected in a sand", *Can. Geotech. J.*, **43**(12), 1273-1289. https://doi.org/10.1139/t06-082.

Schmudderich, C., Shahrabi, M.M., Taiebat, M. and Lavasan, A.A. (2020), "Strategies for numerical simulation of cast-in-place piles under axial loading", *Comput. Geotech.*, **125**, 103656. https://doi.org/10.1016/j.compgeo.2020.103656.

Shrivastava, N. and Zen, K. (2018), "An experimental study of compaction grouting on its densification and confining effects", *Geotech. Geol. Eng.*, **36**(2), 983-993. https://doi.org/10.1007/s10706-017-0369-7.

Silvestri, V. and Abou-Samra, G. (2012), "Analytical solution for undrained plane strain expansion of a cylindrical cavity in modified cam clay", *Geomech. Eng.*, **4**(1), 19-37. https://doi.org/10.12989/gae.2012.4.1.019.

Thiyyakkandi, S., McVay, M., Bloomquist, D. and Lai, P. (2013), "Measured and predicted response of a new jetted and grouted precast pile with membranes in cohesionless soils", *J. Geotech. Geoenviron. Eng.*, **139**(8), 1334-1345. https://doi.org/10.1061/(asce)gt.1943-5606.0000860.

Thiyyakkandi, S., McVay, M., Bloomquist, D. and Lai, P. (2014), "Experimental study, numerical modeling of and axial prediction approach to base grouted drilled shafts in cohesionless soils", *Acta Geotechnica*, **9**(3), 439-454. https://doi.org/10.1007/s11440-013-0246-3.

Wu, Y., Zhang, X.F., Zhao, C. and Zhao, C.F. (2023), "Effects of soil unloading and grouting on the vertical bearing mechanism for compressive piles", *Ocean Eng.*, **271**(2023), 113754. https://doi.org/10.1016/j.oceaneng.2023.113754.

Yang, Z.Q., Hou, K.P. and Guo, T.T. (2011), "Study on the effects of different water-cement ratios on the flow pattern properties of cement grouts", *Proceedings of the International Conference on Green Building, Materials and Civil Engineering (GBMCE 2011)*, August 22-23, Shangri La, China.

Yang, Z.Q., Ding, Y., Mi, Y.P., Zhu, Y.Y., Yang, Y., Guo, Y.H., Zhang, B.H., Li, S.H., Su, J.K., Chen, J.Z., Xu, W.Z., Liu, W.L., Liu, H. and Wang, Y.D. (2021), "Comprehensive effect of the time and water-cement ratio on the rheological properties of power-law cement grouts", *Geofluids*, **2021**, 6636708. https://doi.org/10.1155/2021/6636708.

Zhang, Q.Q., Li, H.T., Cui, W., Zhao, Y.H., Wang, S.L. and Xu, F. (2021), "Analysis of grout diffusion of postgrouting pile considering the time-dependent behavior of grout viscosity", *Int. J. Geomech.*, **21**(11), 04021201. https://doi.org/10.1061/(asce)gm.1943-5622.0002144.

Zhang, Z.M., Zou, J., Liu, J.W. and He, J.Y. (2010), "Theoretical study of climbing height of grout in pile-bottom base grouting", *Rock Soil Mech.*, **31**(8), 2535-2540. (in Chinese)

Zhang, J.Q., Zhao, C.F. and Wu, Y. (2023), "Experimental study on post-grouting pile vertical bearing performance considering different grouting methods and parameters in cohesive soil", *Appl. Sci.*, **13**(22), 12175. https://doi.org/10.3390/app132212175.

Zhao, C.F., Wu, Y., Zhao, C., Zhang, Q.Z., Liu, F.M. and Liu, F. (2019), "Pile side resistance in sands for the unloading effect and modulus degradation", *Materiales De Construccion*, **69**(334), e185. https://doi.org/10.3989/mc.2019.03718.

Zhao, C.F., Wu, Y., Zhao, C. and Wang, Y. (2020), "Load-displacement relationship of single piles in clay considering different tip grouting volumes and grouting returned heights", *Int. J. Geomech.*, **20**(2), 04019158. https://doi.org/10.1061/(asce)gm.1943-5622.0001547.

Zhao, C.F., Zhang, J.Q., Zhao, C., Wu, Y. and Wang, Y.B. (2023), "Cavity reverse expansion considering elastoplastic unloading and application in cast-in-situ bored piles", *Soils Found.*, **63**(2023), 101339. https://doi.org/10.1016/j.sandf.2023.101339.

Zou, J.F., Yang, T. and Deng, D.P. (2019), "Field test of the long-term settlement for the post-grouted pile in the deep-thick soft soil", *Geomech. Eng.*, **19**(2), 115-126. https://doi.org/10.12989/gae.2019.19.2.115.

IC

Notation

The following symbols are used in this paper.

D = pile diameter
E = soil elastic modulus
G = soil shear modulus
h = vertical distance from grout outlet
h_s = distance between grout outlet and soil surface
h_u = ultimate upward diffusion height
K_0 = static soil pressure coefficient
k = grout consistency coefficient
n = rheological index
P = grout pressure
P_0 = initial horizontal soil stress
P_s = initial grouting pressure
P_u = horizontal soil stress after unloading at the drilling wall
q = grout flow rate
v = grout flow velocity
u = reverse radial displacement
y = radial distance between grout center and computed point
Δh = height difference between upper and lower grout section
ΔP = pressure difference between upper and lower grout section
φ = internal friction angle
χ = unloading ratio
γ = shear rate
γ_g = grout weight
γ_m = average weight of soil
γ_{m1} = average weight of soil from grout outlet to soil surface
γ_{m2} = average weight of soil from grout outlet to computed point
δ = thickness of slurry cake
ν = Poisson's ratio
τ = grout shear stress